CFD Modelling of Three-Phase Fluidized Bed with Low Density Solid Particles

In the partial fulfillment of the requirement of

Bachelor of technology

in

Chemical Engineering

Submitted by

Kuldeep Sharma

Roll no. 110CH0087

Under the guidance of

Dr. H.M. Jena

Department of Chemical Engineering

National Institute of Technology

Rourkela-769008

Odisha, India

(May, 2014)

National Institute of Technology

Rourkela

CERTIFICATE

This is to certify that that the work in this thesis report entitled- **CFD modeling of three phase fluidized bed with low density solid particles** -submitted by Kuldeep Sharma in partial fulfillment of the requirements for the degree of Bachelor of Technology in Chemical Engineering Session 2013-2014 in the department of Chemical Engineering, National Institute of Technology Rourkela, Rourkela is an authentic work carried out by him under my supervision and guidance.

Date: -

Dr. H.M.JENA

Department of Chemical engineering

National institute of Technology

Rourkela 769008

ACKNOWLEDGMENT

I owe a debt of deepest gratitude to my thesis supervisor, ***H.M.Jena***, Professor, Department of Chemical Engineering, for his guidance, support, motivation and encouragement throughout the period this work was carried out. His readiness for consultation at all times, his educative comments, his concern and assistance even with practical things have been invaluable**.**

I am sincerely thankful to ***MR.Sambhurisha Mishra*** for acting as my project coordinator and helping me in the learning of software.

I am grateful to Prof. ***R.K.Singh***, Head of the Department, Chemical Engineering for providing us the necessary opportunities for the completion of our project. I also thank the other Staff members of my department for their invaluable help and guidance.

Kuldeep Sharma

Roll no. 110CH0087

4'Th year B.Tech

Department of Chemical engineering

NIT Rourkela

CONTENTS

List of figures and tables

Table no.

ABSTRACT

Three-phase fluidization is defined as an operation in which a bed of solid particles is suspended in gas and liquid media due to net drag force of the gas and/or liquid flowing opposite to the net gravitational force (or buoyancy force) on the particles. Such an operation generates considerable, intimate contact among the gas, liquid and the solid in the system and provides substantial advantages for application in physical, chemical or biochemical processing involving gas, liquid and solid phases. Among all the types of three-phase fluidized beds, three-phase concurrent gas-liquid-solid fluidized beds are used in a wide range of applications including hydro-treating and conversation of heavy petroleum and synthetic crude, coal liquefaction, methanol production, sand filter cleaning, electrolytic timing, conversion of glucose to ethanol, aerobic waste water treatment, and various other hydrogenation and oxidation reactions. The recent fluidized bed bioreactors are superior in performance due to immobilization of cells on solid particles reducing the time of treatment, volume of reactor is extremely small, lack of clogging of bio-mass and removal of pollutant like phenol even at lower concentrations. In the fluidized bed system used in waste water treatment, low density solid matrix is used to immobilize the microbes as the system operates at low water and air velocities to avoid transportation of the particles from the bed. Hydrodynamics study of three-phase fluidized bed with low density particles are rarely seen in literature although a tremendous work is seen for moderate or high density solid particles. In the present work, the computational studies have been carried out on two dimensional fluidized beds to characterize there hydrodynamic behavior. Air, water and low density solid particles have been used as the gas, liquid and solid phase to analyze the system behaviors.

Keywords: *Multiphase, Fluidized bed, CFD, hydrodynamics.*

Nomenclature

β:	Particulate loading, -
α_d:	Volume fraction of discrete phase, -
α_c:	Volume fraction carrier phase, -
ρ_d:	Density of the dispersed phase (*d)*, Kg m^{-3}
ρ_c:	Density of the carrier phase (*c*), kg m^{-3}
St:	Stoke number, -
τ_d:	Particle response time, s
t_s:	System response time, s
d_d:	Diameter of dispersed phase, m
μ_c:	Viscosity of carrier phase, Pa s
L_s:	Characteristics length, m
V_s.:	Characteristic velocity, m s^{-1}
V_q:	Volume of phase q. -
α_q:	Volume fraction of phase q, -
$\vec{\rho}_q$:	Effective density of phase q, Kg m^{-3}
λ_q:	Bulk viscosity of phase *q*, m s^{-1}.
$\vec{F}_q$:	External body force, N
$\vec{F}_{lift,q}$:	Lift force, N
$\vec{F}_{vm,q}$:	Virtual mass force, N
$\vec{R}_{pq}$:	Interaction between phases, -
p :	Pressure, Pa
$\vec{g}$:	Acceleration due to gravity, m s^{-2}

K_{pq} : Fluid-fluid exchange co-efficient, Kg s^{-1}

K_{ls}: Fluid-solid and solid-solid exchange coefficient, Kg s^{-1}

f: Drag function, -

τ_p: Particulate relaxation time, s

μ_p: Viscosity of phase *p*, m s^{-1}.

α_r: Volume fraction of phase *r*, -

μ_r: Viscosity of phase *r*, m s^{-1}.

μ_l: Viscosity of liquid phase, m s^{-1}.

τ_s: Particulate relaxation time, s

d_s : Diameter of the particles of phase *s*, m

α_l: Volume fraction of liquid phase, -

ρ_l: Density of liquid phase, kg m^{-3}

$\vec{v}_l$: Velocity of liquid phase, m s^{-1}

e_{ls}: Coefficient of restitution,-

$C_{fr,ls}$: Coefficient of friction between the l^{th} and s^{th} solid phase particles,-

d_l: Diameter of particle of solid *l*, m

$g_{0,ls}$: Radial distribution coefficient, -.

Θ_s : Granular temperature, K

e_{ss}: Co-efficient of restitution for particle collisions, -

$g_{0,ss}$: Radial distribution function, -

S: Distance between grains, m

μ_s: Solid shear viscosity, m s^{-1}

$\mu_{s,col}$: Collision viscosity, m s^{-1}

$\mu_{s,kin}$: Kinetic viscosity, m s^{-1}

$\mu_{s,fr}$: Frictional viscosity, m s^{-1}

λ_s: Bulk viscosity, m s^{-1}

ϕ: Angle of internal friction, -

K_{Θ_s}: Diffusion co-efficient

Υ_{Θ_s}: Collisional dissipation of energy

Φ_{ls}: Energy exchange between l^{th} solid phase and s^{th}solid phase

$\vec{U}_{s,||}$: Particle slip velocity parallel to the wall, m s^{-1}

ϕ: Specularity co-efficient between particle and wall, -

$\alpha_{s,max}$ Volume fraction for particle at maximum packing, -

$\bar{\bar{\tau}}_q^{"}$: Reynolds stress tensors for continuous phase q, Pa

$\vec{U}_q$: Phase-weighted velocity, m s^{-1}

$\mu_{t,q}$: Turbulent viscosity, Pa s

ε_q: Dissipation rate, m^2 s^{-3}

C_μ: Constant, -

$p_{C_0}^{'}$: Cell pressure correction, Pa

$p^{'}$: Pressure correction, Pa

b : Source term, -

α : Under-relaxation factor, -

α_p: Under relaxation factor for pressure, -

U_{Lmf}: Minimum liquid fluidization velocity, m s^{-}

CHAPTER 1

INTRODUCTION AND LITERATURE SURVEY

Fluidization is an operation by which fine solids are transformed into a fluid-like state through contact with gas or liquid or by both gas and liquid. Gas-liquid-solid fluidization is defined as an operation in which a bed of solid particles is suspended in gas and liquid media due to net drag force of the gas and/or liquid flowing opposite to the net gravitational force (or buoyancy force) on the particles. Such an operation generates considerable, intimate contact among the gas, liquid and the solid in the system and provides substantial advantages for application in physical, chemical or biochemical processing involving gas, liquid and solid phases. Fluidization is broadly of two types, viz. aggregative or bubbling. The gas-liquid-solid fluidization with liquid as continuous phase is of particulate fluidization type, while aggregative fluidization is a characteristic of gas-liquid-solid system with gas as the continuous phase

1.1. Advantages and disadvantages of three-phase fluidized bed:

There are several advantages of fluidized beds such as; ability to maintain a uniform temperature, significantly lower pressure drops which reduce pumping costs, catalyst may be withdrawn, reactivated, and added to fluidized beds continuously without affecting the hydrodynamics performance of the reactor, bed plugging and channeling are minimized due to the movement of solids, high reactant conversion for reaction kinetics, low intra particle diffusion resistance, gas-liquid and liquid-slid mass transfer resistance(shah, 1979; Beaton et al., 1986; Fan, 1989; Le Page et al., 1992; Jena, 2010). There are, however, also some disadvantages to fluidized beds such as; catalyst attrition due to particle motion, entrainment and carryover of particles, relatively larger reactor size compared to bed expansion, not suitable for reaction kinetics favoring plug flow pattern, low controllability over product selectivity for complex reaction and loss of driving force due to back mixing of particles in case transfer operations (Jena, 2010)

1.2. Application of three-phase fluidized bed:

Among all the types of three-phase fluidized beds, three-phase concurrent gas-liquid-solid fluidized beds are used in a wide range of applications including hydro-treating and conversation of heavy petroleum and synthetic crude, coal liquefaction, methanol production, sand filter cleaning, electrolytic timing, conversion of glucose to ethanol, aerobic waste water

treatment, and various other hydrogenation and oxidation reactions (Fan, 1989; Wild and Poncin, 1996; Jena, 2010).

1.3. Hydrodynamic studies of three-phase fluidized beds with low density particles:

Low density solid particles found huge application in bio reactor for aerobic waste water treatment. Hydrodynamics study of three-phase fluidized bed with low density particles are rarely seen in literature although a tremendous work is seen for moderate or high density solid particles. Hydrodynamics of a gas-liquid-solid fluidized bed with low density solid [Kaldnes Miljotechnologies AS (KMS)] support was investigated by Sokół and Halfani (1999), they have found that value of minimum fluidization air velocity depend on the ratio of bed to reactor volume and mass of cell growth on the particles. The effect of operational parameters on biodegradation of organics in fluidized bed bioreactor with low density solid particles have been studied by Sokół (2001) and Sokół and Korpal (2004). Briens and Ellis (2005) have characterized the hydrodynamics of three-phase fluidized bed systems by statistical, fractal, chaos and wavelet analysis. The solid particles covered with a biofilm are fluidized by air and contaminated water by Allia et al. (2006) to confirm the operating stability, to identify the nature of mode flow and to determine some hydrodynamic parameters such as the minimum fluidization velocity, the pressure drop, the expansion, the bed porosity, the gas retention and the stirring velocity

Even though a large number of experimental studies are directed towards the quantification of flow structure and flow regimes identification for different process parameters and physical properties, the complex hydrodynamics of these reactor are not well understood due to complicated phenomena such as particle-particle, liquid-particle, and particle-particle interactions (Jena, 2010). As regard to mathematical modeling, computational fluid dynamics (CFD) simulation give detailed information about the local values of pressure, viscous and turbulent stresses, turbulent kinetics energy and turbulent energy dissipation rate, etc.

1.4. Computational fluid dynamic studies on three-phase fluidized beds:

Recently, several CFD models based on Eulerian multi-fluid approach have been developed for gas–liquid-solid flows (Matonis et al., 2002; Feng et al., 2005; Schallenberg et al., 2005). Grevskott et al. (1996) have carried out computational fluid dynamic simulation of three phase slurry reactor by two fluid models, with the two phases treated in an Eulerian frame of reference. The inter-phase momentum exchange terms modeled between the fluid phases were steady interfacial drag, added mass force and lift force. They have also tested a new model for bubble size distribution and solid pressure. Their new bubble size model is found to improve

the size distribution prediction compared to prior model. Mitra-Majumdar et al. (1997) have used computational fluid dynamics model to examine the structure of three-phase (air-water-glass beads) flow through a vertical column. In their study they proposed new co-relation to modify the drag between the liquid and the gas phase to account for the effect of solid particles on bubble motion. They have used K- ϵ model for simulating the effect of turbulence on the flow field. Jianping and Shonglin (1998) have used a two dimensional pseudo-two phase fluid dynamics model with turbulence calculate local values of axial liquid velocity and gas holdup in a concurrent gas-liquid-solid three-phase bubble column reactor. They have concluded that local axial liquid velocity and local gas holdup value are strongly influenced by solid loading and operating condition, local gas holdup and axial liquid velocity increased as the solid loading declined and under certain circumstance.

Li et al. (1999) have carried out CFD simulation of gas bubbles rising in water in a small two dimensional bed glass beads. They have applied a bubble induced force model, continuum surface force model and Newton third law respectively for the couplings of particle-bubbles, gas-liquid and particle liquid interactions. It is shown that their model can capture the bubble wake behavior such as wake structure and the shedding frequency. Zhang et al. (2000a) have conducted a discrete phase simulation to study the bubble and particle dynamics in a three phase fluidized bed at high pressure. They have employed the Eulerian volume-averaged method, the Lagrangian dispersed particle method, and the volume of fluid (VOF) method to describe the motion of liquid, solid particles, and gas bubbles. Zhang et al. (2000b) have developed a computational scheme for discrete-phase simulation of a gas-liquid-solid fluidization system and a two-dimensional code based on it. The volume-averaged method, the dispersed particle method, and the volume-of-fluid (VOF) method have been used to account for the flow of liquid, solid particles, and gas bubbles respectively.

Padial et al. (2000) have used finite-volume flow simulation technique to study the three dimensional simulation of three phase flow in a conical-bottom draft-tube bubble column. They have employed an unstructured grid method along with a multifield description of the multiphase flow dynamics. They have observed the same loss of column circulation as experimental when the column is operated with the draft tube in its highest position. Li et al. (2001) have conducted a discrete phase simulation (DPS) to investigate multi-bubble formation dynamics in gas-liquid-solid fluidization systems. They have developed and employed a numerical technique based on computational fluid dynamics (CFD) with the discrete particle method (DPM) and volume tracking represented by the volume-of-fluid (VOF) method for simulation. They have applied a bubble-induced force (BIF) model, a continuum surface force

(CSF) model, and Newton's third law to account for the couplings of particle-bubble, bubble-liquid and particle-liquid interactions, respectively. Matonis et al. (2002) have developed experimentally verified computational fluid dynamic model for gas-liquid-solid flow. A three-dimensional transient computational code for the coupled Navier-Strokes equations for each phase has been used. Their simulation shows a down flow of particles in the center of the column, and an up flow near the wall, and a nearly uniform particle concentration. Chen and Fan (2004) have developed two dimensional Eulerian–Lagrangian model for three-phase Fluidization and used Level-set method for interface tracking and Sub-Grid Scale (SGS) stress model for bubble-induced turbulence to characterize the bubble rise velocity, bubble shapes and their fluctuations, and bubble formation. Glover and Generalis (2004) have presented an alternate approach to the modeling of solid-liquid and gas-liquid-solid flow for a 5:1 height to width ratio bubble column. Feng et al. (2005) have developed a 3-dimensional computational fluid dynamics (CFD) model to simulate the structure of gas-liquid-TiO2 nanoparticles three-phase flow in a bubble column. The have been compared with experimental data for model validation.

Wiemann and Mewes (2005) have presented a numerical method for the calculation of the three- dimensional flow fields in bubble columns based on a multi fluid model. They have obtained the local and the integrated volume fraction of gas in the bed from CFD simulation. Zhang and Ahmadi (2005) have used an Eulerian-Lagrangian computational model for simulation of gas-liquid-solids flows in three phase slurry reactors. They have used a volume-averaged system of governing equations for liquid flow model whereas motion of bubbles and particles are evaluated by the Lagrangian trajectory analysis procedure. The simulation result shows dominance of time-dependent staggered vortices on the transient characteristics. The bubble size significantly affects the characteristics of three-phase flows and flows with larger bubbles appear to evolve faster.

Annaland et al. (2005) has presented a hybrid model for the numerical simulation of gas-liquid-solid flow using a combine front tracking (FT) for dispersed gas bubbles and solid particle present in the continuous liquid phase. In addition they have quantified the retarding effect on bubble rising velocity due to presence of suspended solid particles. Schallenberg et al. (2005) have used a computational fluid dynamic model to calculate a three-phase (air-water-solid particles) flow in a bubble column. They have used the K-ε turbulence model extended with term accounting for the bubble-induced turbulence to calculate the eddy viscosity of the liquid phase. They have observed good agreement between the measured and the calculated results.

Cao et al. (2009) have modeled gas-liquid-solid circulating fluidized bed by two dimensional, Eulerian–Eulerian–Lagrangian (E/E/L) approaches. E/E/L model combined with Two Fluid Model (TFM) and Distinct Element Method (DEM). Based on generalized gas–liquid two fluids *k-ε* model, the modified gas–liquid TFM is established. Muthiah et al. (2009) have carried out computational fluid dynamics to characterize the dynamics of three-phase flow in cylindrical fluidized bed, run under homogeneous bubble flow and heterogeneous flow condition. They observed that higher gas velocity, higher value of solid loading and lower particles diameter make the system diameter faster.

O'Rourke et al. (2009) have developed 3D model and used Eulerian finite difference approach to simulate gas-liquid-solid fluidized bed. The mathematical model using multiphase particle-in-cell (MP-PIC) method is used for calculating particle dynamics (collisional exchange) in the computational-particle fluid dynamics (CPFD). Paneerselvam et al. (2009) have developed a three dimensional transient model to simulate the local hydrodynamics of a gas-liquid-solid three phase fluidized bed reactor using the CFD method. From the validated CFD model, they carried out the computation of the solid mass balance and various energy flows in fluidized bed reactors.

Sivaguru et al. (2009) have carried out the CFD analysis of three-phase fluidized bed to predict the hydrodynamics. They have taken liquid phase as water that continuously flow, whereas the gas phase is air which flow discretely throughout the bed. They have obtained the simulation result using porous jump and porous zone model to represent the distributor. They have found that porous zone model is best applicable in Industries, since stability of operating condition is achieved even with non-uniform air, water flow rate and with different bed height. Nguyen et al. (2011) have carried out CFD simulation using commercial CFD package FLUENT 6.2 to understand the hydrodynamics of three phase fluidized bed. They have investigated the complex hydrodynamics of three phase fluidized bed such as bed expansion, holdup for two phases, bed pressure drop, and fluidized bed voidage and velocity profile. They have used Euler-Euler multiphase approach for predicting the overall performance of gas –liquid-solid fluidized bed and Gidaspow model is used as drag model for simulation.

Hamidpour et al (2012) have performed CFD simulations of gas-liquid-solid fluidized beds in a full three dimensional, unsteady multiple-Euler frame work by mean of the commercial software FLUENT. They have investigated the significance of implementing accurate numerical schemes as well as the choice of available K-ε turbulence models (standard, RNG, realizable), solid wall boundary condition and granular temperature model. The result indicated

that in order to minimize numerical diffusion artifacts and to enable valid discussions on the choice of physical models, third order numerical schemes need to be implemented.

The report on the computational models for the hydrodynamics characteristics of three-phase fluidized bed is limited. Most of these CFD studies are based on steady state, 2D axisymmetric, Eulerian multi-fluid approach. But in general, three phase flows in fluidized bed reactors are intrinsically unsteady and are composed of several flow processes occurring at different time and length scales. The unsteady fluid dynamics often govern the mixing and transport processes and is inter-related in a complex way with the design and the operating parameters like reactor and sparger configuration, gas flow rate and solid loading. Computational model of 0.10m diameter and 1.88 m height column have been studied with changing gas and liquid velocity. Changing inlet conditions will change the flow characteristics. The hydrodynamic study of three-phase fluidized bed is meager and very less amount of content of literature available to describes the hydrodynamic study of low density particles in a three phase fluidized bed by CFD simulation Thus the present work has been carried out with the following main objectives.

1.5. Research objectives:

The main objectives of the present research work are summarized below:

- Hydrodynamic study on three-phase fluidized bed with low density particles (propylene beads) using water and air as liquid and gas phase.
- To studied the grid independency for fluidized bed model.
- To studied the effect of different viscous model on hydrodynamics properties

1.6. Thesis summary:

This thesis comprises of five chapters v.i.z. Introduction and Literature Survey, Experimental setup and technique, Computational Flow Model and Numerical Methodology, Result and Discussion and Conclusion and Future scope of the work.

- *Chapter 1*, the background information, literature review and objective of the present work is discussed.
- *Chapter 2* deals with the computational models, the numerical methods, mesh quality, boundary condition, material description etc. used in the CFD simulation.
- *Chapter 3* the results of various hydrodynamics properties obtained from the simulation have represented graphically and discussed.
- *Chapter 4* deals with overall conclusion. Future recommendations based on the research outcome are suggested. The major findings of the work are also summarized.

CHAPTER 2

COMPUTATIONAL FLOW MODEL AND NUMERICAL METHODOLOGY

CFD is a powerful tool for the prediction of the fluid dynamics in various types of systems, thus, enabling a proper design of such systems. The Finite Volume Method (FVM) is one of the most versatile discrimination techniques used for solving the governing equations for fluid flow. The most compelling features of the FVM are that the resulting solution satisfies the conservation of quantities such as mass and momentum. In the finite volume method, the solution domain is subdivided into continuous cells or control volumes where the variable of interest is located at the centroid of the control volume forming a grid. There are several schemes that can be used for discretization of governing equations e.g. central differencing, upwind differencing, power-law differencing and quadratic upwind differencing schemes. The resulting equation is called the discretized equation.

In the present work three geometries of a physical unit has been considered. First a two dimensional (2D) geometry without distributor is simulated with CFD tools to check the present findings with previous ones available which are mostly based on two 2D models. Commercial CFD package ANSYS FLUENT has been used in modeling and simulation of various geometries considered.

Three-phase fluidization involve gas, liquid and solid phases, hence for computational study choosing of appropriate multiphase model play an important role in the simulation result. There are different multiphase models available in commercial software ANSYS FLUENT. In the present work a series of computational models available in FLUENT have been used. The details of various models and numerical schemes used in the present work are discussed in this chapter.

2.1. Computational model for multiphase flow:

Advance in computational fluid mechanics have provided the basis for further insight into the dynamics of multiphase flow. For volume averaged information on any hydrodynamic property the Euler-Euler approach is suitable for its simplicity. Conservation equations for each phase are derived to obtain a set of equations which have similar structure for all phase. The equations are closed by providing constitutive relations that are obtained from empirical information or in the case of granular flow by application of kinetic theory.

The Eulerian model is the most complex of the multiphase model. It solves a set of *n* momentum and continuity equations for each phase. Through the pressure and interphase exchange coefficients coupling are achieved. The manner in which this coupling is handled depends upon the type of phases involved; granular (fluid solid) flows are handled differently than non-regular (fluid-fluid) flows. For granular flows, the properties are obtained from the application of kinetic theory. Momentum exchange between the phases is also depends upon the type of mixture being modeled. The Reynolds Stress turbulence model is not available on a per phase basis, inviscid flow is not allowed, melting and solidification are not allowed, and Particle tracking (using the Lagrangian dispersed phase model) interacts only with the primary phase. Streamwise periodic flow with specified mass flow rate cannot be modeled when the Eulerian model is used, and when tracking particles in parallel, the DPM model cannot be used with the Eulerian multiphase model if the shared memory option is enabled.

2.2. Conservation equations:

The motion of each phase is governed by respective mass and momentum conservation equations.

Conservation of mass:

$$\frac{\partial}{\partial t}\left(\alpha_q \rho_q\right) + \nabla.\left(\alpha_q \rho_q \vec{v}_q\right) = 0 \qquad (2.1)$$

Where ρ_q is the density of the phase, $\alpha_q$is the volume fraction and $\vec{v}_q$is the volume fraction of the phase $q = L, g, s$. The volume fraction of the three phases satisfies the flowing condition:

$$\alpha_L + \alpha_g + \alpha_s = 1 \qquad (2.2)$$

Conservation of momentum: The conservation of momentum equation for the fluid phase is

$$\frac{\partial}{\partial t}\left(\alpha_q \rho_q \vec{v}_q\right) + \nabla.\left(\alpha_q \rho_q \vec{v}_q \vec{v}_q\right) = -\alpha_q \nabla p + \nabla.\bar{\bar{\tau}}_q + \alpha_q \rho_q \vec{g} + \vec{F}_{i,q} \qquad (2.3)$$

Where q is for liquid and gas phases, $\bar{\bar{\tau}}_q$ is the stress-strains tensor of liquid and gas phase and $\vec{g}$ is the acceleration due to gravity.

The conservation of momentum for the solid phase is

$$\frac{\partial}{\partial t}(\alpha_s \rho_s \vec{v}_s) + \nabla.(\alpha_s \rho_s \vec{v}_s \vec{v}_s) = -\alpha_s \nabla p - \nabla.p_s + \nabla.\bar{\bar{\tau}}_s + \alpha_s \rho_s \vec{g} + \vec{F}_{i,s} \qquad (2.4)$$

Where $p_s$the sth is solid pressure, and $\bar{\bar{\tau}}_s$is the stress-strains tensor of solid phase.

$$\bar{\bar{\tau}}_q = \alpha_q \mu_q \left(\nabla . \vec{v}_q + \nabla . \vec{v}_q^T\right) + \alpha_q \left(\lambda_q - \frac{2}{3}\mu_q\right) \nabla . \vec{v}_q \bar{\bar{I}} \quad (2.5)$$

$$\bar{\bar{\tau}}_s = \alpha_s \mu_s (\nabla . \vec{v}_s + \nabla . \vec{v}_s^T) + \alpha_s \left(\lambda_s - \frac{2}{3}\mu_s\right) \nabla . \vec{v}_s \bar{\bar{I}} \quad (2.6)$$

2.2.1. Interphase Exchange Co-efficient:

The inter phase momentum exchange terms F_i are composed of a linear combination of different interaction forces between different phases such as the drag force, the lift force and the added mass force, etc., and is generally represented as

$$F_i = F_D + F_L + F_M \quad (2.7)$$

The lift force is insignificant compared to the drag force. Hence, only the drag force is included for inter-phase momentum exchange in the present CFD simulation. The inter-phase force depends on the friction, pressure, cohesion and other effects and is subject to the conditions that $F_{D,jk} = -F_{D,kj}$ and$F_{D,jj} = 0$, where, subscripts *j* and *k* represent various phases. The inter-phase force term is defined as:

$$F_{D,jk} = K_{jk}\left(u_j - u_k\right) \quad (2.8)$$

Where $K_{jk}\left(= K_{kj}\right)$ is the inter-phase momentum exchange coefficient.

In the present work, the liquid phase is considered as a continuous phase and both the gas and the solid phases are treated as dispersed phases. The inter phase drag force between the phases is discussed below.

Fluid-fluid exchange co-efficient: For fluid-fluid flow, each secondary phase is assumed to form droplets or bubbles. This exchange co-efficient can be written in the following general form.

$$K_{pq} = \frac{\alpha_q \alpha_p \rho_p f}{\tau_p} \quad (2.9)$$

Where f is the drag function, is defined differently for the different exchange co-efficient models andτ_p, the "particulate relaxation time", is defined as

$$\tau_p = \frac{\rho_p d_p^2}{18\,\mu_q} \quad (2.10)$$

Where d_p is the diameter of the bubbles or droplets of phase *p***.** Nearly all definition of *f* include a drag co-efficient *(* C_D) that is based on the relative Reynolds number (*Re*). It is the drag

function that differs among the exchange co-efficient models. For all these situations, K_{pq} should trend to zero. Whenever the primary phase is not present with in the domain, to enforce this *f* is always multiplied by the volume fraction of the primary phase *q* as shown in equation (2.11).

In the present model we have used Schiller and Naumann model to define the drag function *f*.

$$f = \frac{C_D Re}{24} \tag{2.11}$$

Where $C_D = 24\,(1 + 0.15\,Re^{0.687})/\,Re \qquad Re \leq 1000$

$$C_D = 0.44 \qquad Re \geq 1000$$

And *Re* is the relative Reynolds number. The relative Reynolds number for the primary phase *q* and secondary phase is obtained from

$$Re = \frac{\rho_{rp}|\vec{v}_r - \vec{v}_p|d_{rp}}{\mu_{rp}} \tag{2.12}$$

Where $\mu_{rp} = \alpha_p\mu_p + \alpha_r\mu_r$ is the mixture viscosity of the phase *p* and *r*.

Fluid-solid Exchange Co-efficient: The fluid-solid exchange co-efficient K_{sl} can be written in the following general form.

$$K_{sl} = \frac{\alpha_s\rho_s f}{\tau_s} \tag{2.13}$$

Where *f* is defined differently for the different exchange co-efficient model andτ_s**,** the particulate relaxation time.

$$\tau_s = \frac{\rho_s d_s^2}{18\,\mu_l} \tag{2.14}$$

Where d_s is the diameter of the particles of phase *s.* All definition of *f* includes a drag function (C_D) that is based on the relative Reynolds number (Re_s). It is this drag function that differs among the exchange co-efficient models.

In our present study, we have taken Gidaspow model, combination of Wen and Yu model and the Ergun equation.

When$\alpha_l > 0.8$**,** the fluid solid exchange coefficient K_{sl} is of the following form:

$$K_{sl} = \frac{3}{4} C_D \frac{\alpha_s \alpha_l \rho_l |\vec{v}_s - \vec{v}_l|}{d_s} \alpha_l^{-2.65} \quad (2.15)$$

Where $$C_D = \frac{24}{\alpha_l Re_s} [\, 1 + 0.15(\alpha_l Re_s)^{0.687}] \quad (2.16)$$

Where Re_s is defined as,

$$Re_s = \frac{\rho_l d_s |\vec{v}_s - \vec{v}_l|}{\mu_l} \quad (2.17)$$

l is the l^{th} fluid phase, s is for the s^{th} solid phase particles and d_s is the diameter of the s^{th} solid phase particles

When$\alpha_l \leq 0.8$,

$$K_{ls} = \frac{3(\,1 + e_{ls}) \left(\frac{\pi}{2} + C_{fr,ls} \frac{\pi^2}{8}\right) . \alpha_s \rho_s \alpha_l \rho_l (d_l + d_s)^2 g_{0,ls} |\vec{v}_l - \vec{v}_s|}{2\pi(\rho_l d_l^3 + \rho_s d_s^3)} \quad (2.18)$$

Where e_{ls}= the coefficient of restitution

$C_{fr,ls}$= the coefficient of friction between the l^{th} and s^{th} solid phase particles.

d_l = diameter of the particle of solid l

$g_{0,ls}$ = the radial distribution coefficient.

2.3. Closure law for solid pressure:

For granular flow in the compressible regime (i.e. where the solid volume fraction is less than its maximum allow value), a solid pressure is calculated independently and used for the pressure gradient term,$\nabla . p_s$, in the granular-phase momentum equation. Because a Maxwellian velocity distribution used for the particles, a granular temperature is introduced into the model, and appears in the expression for the solid pressure and viscosities. The solid pressure is composed of a kinetic term and a secondary term due to particle collisions.

$$p_s = \alpha_s \rho_s \Theta_s + 2\rho_s (1 + e_{ss}) \alpha_s^2 g_{0,ss} \Theta_s \quad (2.19)$$

Where e_{ss} is the co-efficient of restitution for particle collisions, $g_{0,ss}$ is the radial distribution function, and Θ_s is the granular temperature. The granular temperature Θ_s is proportional to the kinetic energy of the fluctuating particle motion. In ANSYS FLUENT a default value of 0.9 for Θ_s is use and can be adjusted to suit the particle type. The function $g_{0,ss}$ is a distribution function that governs the transition from the "compressible" condition with $\alpha_s < \alpha_{s,max}$,

where the spacing between the solid particles can continue to decrease, to incompressible condition with $\alpha = \alpha_{s,max}$, where no further decrease in space can occurs. The value of 0.63 is the default for$\alpha_{s,max}$.

2.4. Closure law for turbulence:

To describe the effect of turbulent fluctuation of velocities in a multiphase flow, the number of terms to be modeled in the momentum equations is large, and this make the modeling of turbulence in multiphase simulations extremely complex. There are three methods for modeling turbulence in multiphase flow mixture turbulence model, dispersed turbulence model and turbulence model for each phase. In the present work dispersed turbulence model is applied.

$K-\varepsilon$ Dispersed model: This model is applicable only when there is clearly one primary continuous phase and rest are dispersed dilute secondary phases. In this case, interparticle collision collisions are negligible and the dominant process in the random motion of the secondary phase is the influence of the primary phase turbulence. Fluctuating quantities of the secondary phases can therefore be given in term of the mean characteristics of the primary phase and the ratio of the mean particle relaxation time and eddy-particle relaxation time.

Turbulent prediction are obtained from the modified $K-\varepsilon$ model

$$\frac{\partial}{\partial t}\left(\alpha_q \rho_q k_q\right) + \nabla.\left(\alpha_q \rho_q \vec{U}_q k_q\right) = \nabla.\left(\alpha_q \frac{\mu_{t,q}}{\sigma_k} \nabla k_q\right) + \alpha_q \rho_q \varepsilon_q + \alpha_q \rho_q \Pi_{k_q} \qquad (2.20)$$

And

$$\frac{\partial}{\partial t}\left(\alpha_q \rho_q \varepsilon_q\right) + \nabla.\left(\alpha_q \rho_q \vec{U}_q k_q\right) = \nabla.\left(\alpha_q \frac{\mu_{t,q}}{\sigma_\varepsilon} \nabla \varepsilon_q\right) + \alpha_q \frac{\varepsilon_q}{k_q}\left(C_{1\varepsilon} G_{k,q} - C_{2\varepsilon} \rho_q \varepsilon_q\right) + \alpha_q \rho_q \Pi_{\varepsilon_q} \qquad (2.21)$$

Here $\Pi_{k_q}$and Π_{ε_q}represent the influence the dispersed phase on the continuous phase q, and $G_{k,q}$ is production of turbulence kinetic energy.

The term $\Pi_{k_q}$is derived from the instantaneous equation of the continuous phase and takes the following form, where M represent the number of secondary phases.

$$\Pi_{kq} = \sum_{p=1}^{M} \frac{k_{pq}}{\alpha_q \rho_q}\left(k_{pq} - 2k_q + \vec{v}_{pq}.\vec{v}_{dr}\right) \qquad (2.31)$$

Turbulence in dispersed phase: Time and length scale which characterize the motion are used to evaluate dispersion co-efficient correlation functions, and the turbulent kinetic energy of each dispersed phase.

The characteristic relaxation time connected with inertial effects acting on a dispersed phase p is defined as

$$\tau_{F,pq} = \alpha_p \rho_q K_{pq}^{-1} \left(\frac{\rho_p}{\rho_q} + C_v \right) \tag{2.32}$$

The Lagrangian integral time scale calculated along the particle trajectories, mainly affected by the crossing trajectories, mainly effect, is defined as

$$\tau_{t,pq} = \frac{\tau_{t.q}}{\sqrt{(1 + C_\beta \xi^2}} \tag{2.33}$$

Where

$$\xi = \frac{\left|\vec{v}_{pq}\right| \tau_{t,q}}{L_{t,q}} \tag{2.34}$$

And

$$C_\beta = 1.8 - 1.35(cos\,\theta)^2 \tag{2.35}$$

Where θ is the angle between the mean particle velocity and the mean relative velocity.

The ratio between these characteristic times is written as,

$$\eta_{pq} = \frac{\tau_{t,pq}}{\tau_{F,pq}} \tag{2.36}$$

Turbulence quantities for dispersed phase *p* as

$$k_p = k_q \left(\frac{b^2 + \eta_{pq}}{1 + \eta_{pq}} \right) \tag{2.37}$$

$$k_{pq} = 2k_q \left(\frac{b + \eta_{pq}}{1 + \eta_{pq}} \right) \tag{2.38}$$

$$D_{t,pq} = \frac{1}{3} k_{pq} \tau_{t,pq} \tag{2.39}$$

$$D_p = D_{t,pq} + \left(\frac{2}{3} k_p - b \frac{1}{3} k_{pq} \right) \tau_{F,pq} \tag{2.40}$$

$$b = (1 + C_v) \left(\frac{\rho_p}{\rho_q} + C_v \right) \tag{2.41}$$

And C_v = 0.5 is the added mass coefficient.

2.5. Numerical Methodology:

In ANSYS FLUENT control-volume based technique is used to convert a general scalar transport equation to an algebraic equation that is solved numerically. This control volume technique consists of integrating the transport equation about each control volume, resulting in a discrete equation that expresses the conservation law on a control-volume basis.

2.5.1. Geometry and Mesh:

Two numbers of two dimensional computational geometries, one without distributor and the other with distributor and a three dimensional computational geometry without distributor of the fluidization column have been generated by using DESIGN MODELLER available in ANSYS software. Fig.2.1. shows the line diagram of the fluidized beds used in simulation. After the creation of geometry of the fluidized bed meshing has been done for each of the geometry. The meshes of various geometries are shown in Fig. 3.4. Detail of the type, size and number of elements with different computational meshes are listed in the Table 2.1.

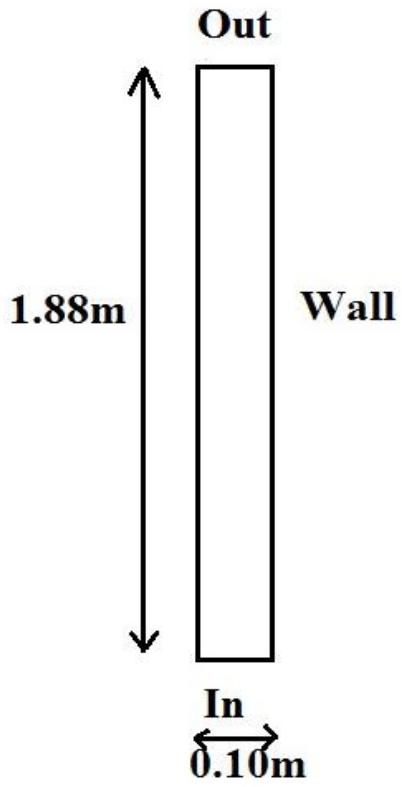

Fig. 2.1. Line diagram of computational geometry fluidized bed

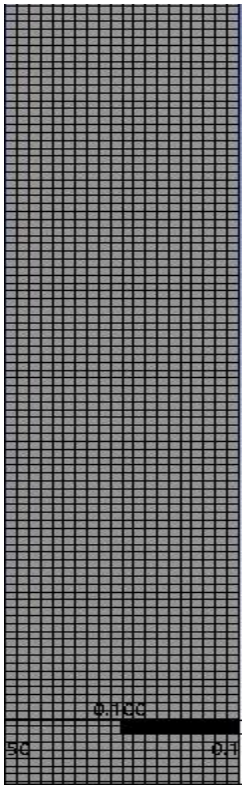

Fig. 2.2. 2D mesh generated in meshing

Table 2.1. Meshing configuration used in the computations of fluidized bed

2D fluidized bed		
Mesh type	Quadrilateral mesh	
Element size	0.005 m	0.0075
Number of Node	15834	18574
Number of Element	7520	9250

2.5.2. Boundary and initial conditions:

In order to obtain a well-posed system of equations, reasonable boundary conditions for the computational domain have to be implemented. Inlet boundary condition is a uniform liquid and gas velocity at the inlet, and outlet boundary condition is the pressure boundary condition, which is set as 1.013×105 Pa. Wall boundary conditions are no-slip boundary conditions for the liquid phase and free slip boundary conditions for the solid phase and the gas phase. The higher viscous effect and higher velocity gradient near the wall have been dealt with the standard wall function method. At initial condition the solid volume fraction of 0.55 for polypropylene beads of the static bed height of column has been used and the volume fraction

of the gas at the inlet and in the free board region is based on the inventory. Table 2.2 represents the detail description of the boundary and initial conditions used in simulation.

Table 2.2. Description of systems used in simulation

Diameter of column:	0.1 m
Height of column:	1.88 m
Solid phase	Polypropylene beads
Particle size, mm:	8
Particle density, Kg/m^3:	1133
Superficial liquid velocity:	0.01 to 0.06 m/s
Static bed voidage:	0.247
Superficial gas velocity:	0.003 to 0.006 m/s
Liquid phase (water), 300˚C	
Viscosity, Pas:	$7.98x10^{-4}$
Density, Kg/m^3:	995.7
Gas phase (air), 300˚C	
Viscosity, Pas:	$1.794x10^{-5}$
Density, Kg/m^3:	1.166

CHAPTER 3

RESULT AND DISCUSSION

In the present work attempt has been made to study the effect of grid size (0.005 m and 0.074 m) and viscous model (Laminar and K-Epsilon Model) on hydrodynamics behavior of three phase fluidized bed with low density solid particles. Result obtained were discussed below.

Bed pressure drop: Fig 3.1 shows that the bed pressure drop depends upon both gas and liquid velocity. The observations have been seen that bed pressure drop increases when gas velocity increases. At constant water velocity, the bed pressure drop decreases as gas velocity increased. When gas velocity is very low there has been very less change in bed pressure drop because at very low gas velocity the fluidization process behave like solid-liquid fluidization. As we increases the superficial liquid velocity at constant gas velocity, initially there have been some increment in the bed pressure drop but when the process tends to steady state, the rate of change of bed pressure drop tends to zero.

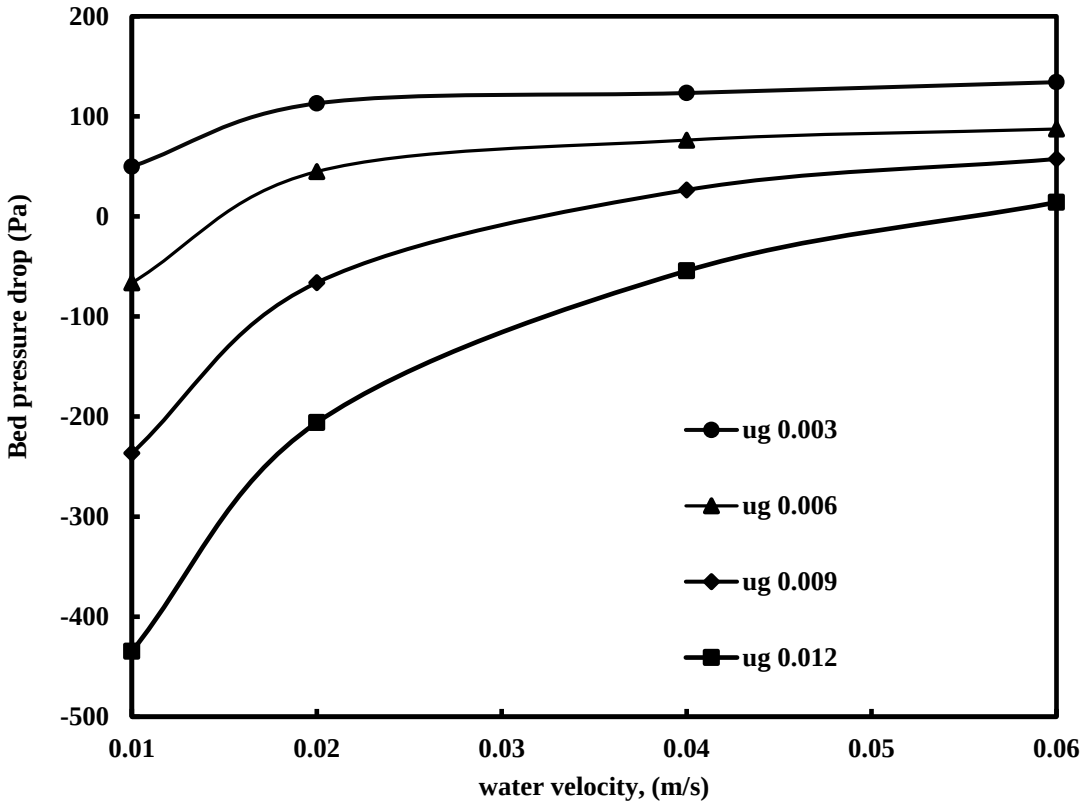

Fig.3.1. Variation of bed pressure drop (Pa) with liquid velocity (m/s) at constant air velocities (m/s) for 8 mm Polypropylene beads at Hs= 0.247 m and grid size 0.0075m using laminar model.

In fig 3.2 shows that the behaviour of bed pressure drop in the fluidized column having 0.005m as grid size with step change (0.01 m/s) in the liquid velocity at constant gas velocity the following graph gives us the idea that at lower velocity (0.003 m/s) the variation of bed pressure drop gives nearly straight line graph and the curve behaviour of the bed pressure drop can be found by increasing gas velocity.

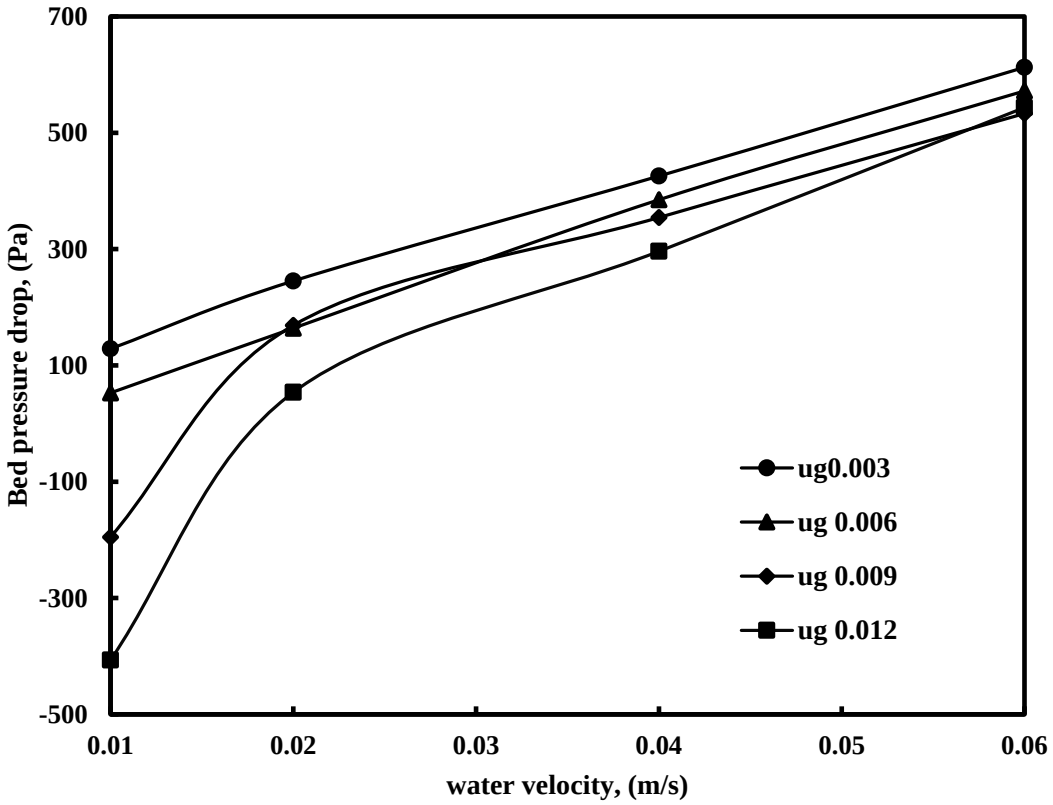

Fig 3.2Variation of bed pressure drop (Pa) with liquid velocity (m/s) at constant air velocities (m/s) for 8 mm Polypropylene beads at Hs= 0.247 m and grid size 0.005m using laminar model.

Fig 3.3 and fig 3.4 shows us the comparison of bed pressure drop to laminar and turbulent model.at different grid size (0.005 and 0.0075m) It has been seen that the at particular gas velocity the laminar and turbulent model behaves quite similarly. At particular constant gas velocity (0.003 and 0.006 m/s) the laminar and turbulent model phenomena shows the overlapping which defines that we can choose any model either laminar or turbulent for the current case. In the grid size of 0.005m the bed pressure drop gives straight line behaviour rather than the grid size 0.0075m which shows curve behaviour. Fig 3.4 shows that at higher liquid velocity bed pressure drop line becomes more and more stagnant.

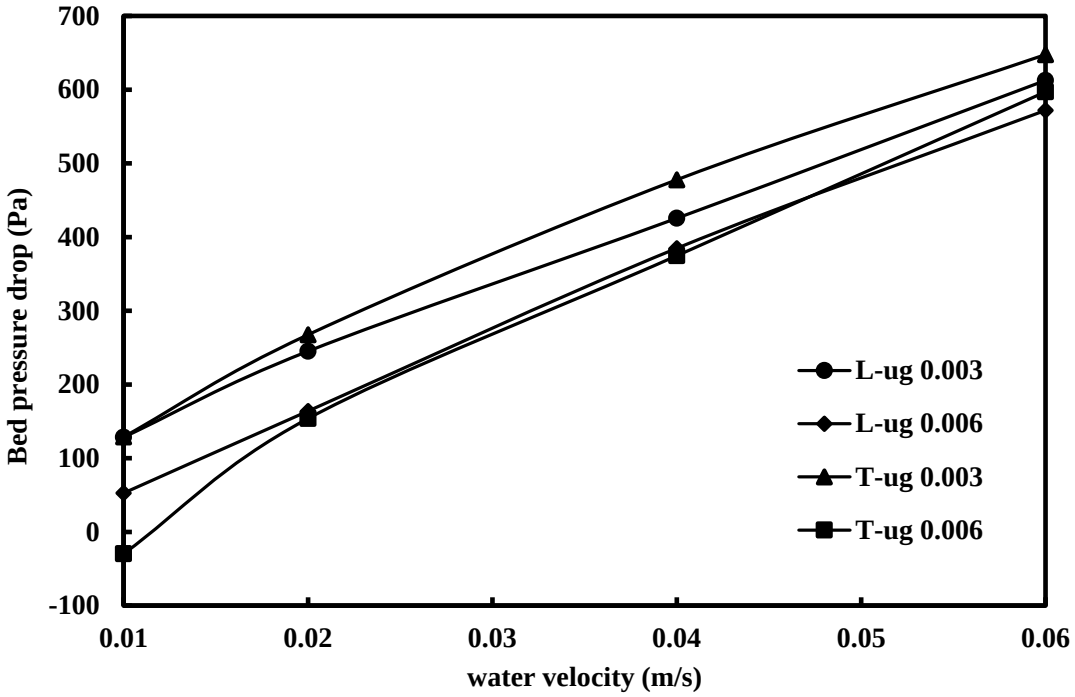

Fig 3.3 Comparison of bed pressure drop (Pa) between laminar and turbulent model with liquid velocity (0.01 to 0.06m/s) at constant air velocities (m/s) for 8 mm Polypropylene beads at Hs= 0.247 m and grid size 0.005m.

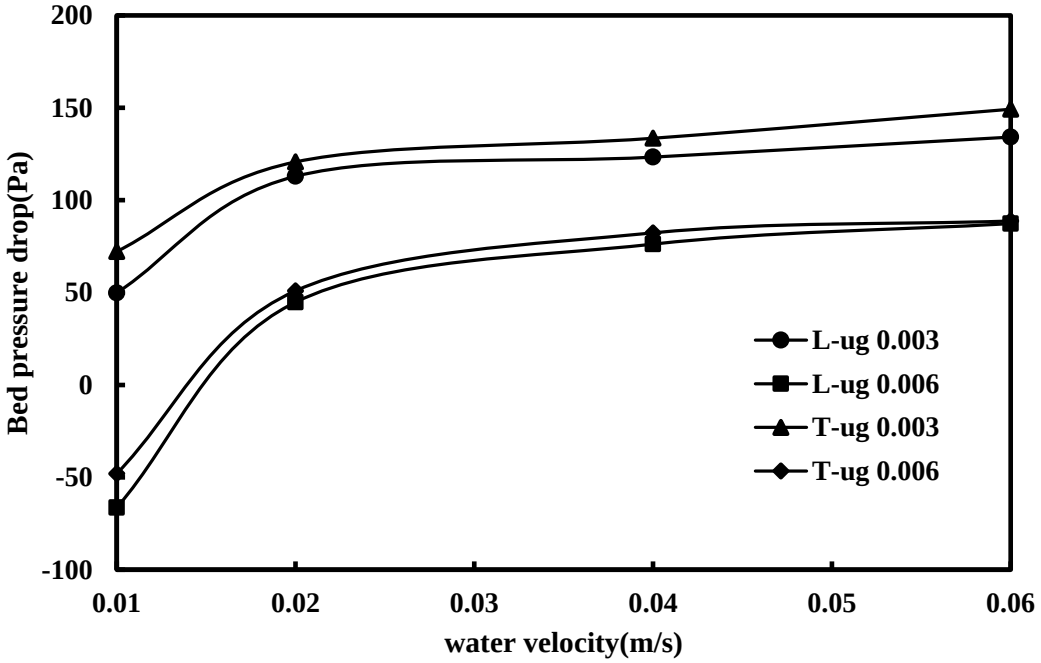

Fig 3.4 Comparison of bed pressure drop (Pa) between laminar and turbulent model with liquid velocity (0.01 to 0.06m/s) at constant air velocities (m/s) for 8 mm Polypropylene beads at Hs= 0.247 m and grid size 0.0075m.

Gas holdup: Gas holdup is obtained as mean-area weighted average of volume fraction of air at sufficient number of points in the fluidized part of the bed. Since the volume fraction of air phase is not the same at all points in the fluidized part of the column, hence an area weighted average of volume fraction of air determined at regular height till the fluidized part is over. When these values are averaged it gives the required gas holdup. The following fig 3.5 and 3.6 shows that the gas hold up value has been decreasing due to increasing in water velocity at constant gas velocity. It also shows that the gas hold up value increases in the increment of gas velocity at constant liquid velocity.

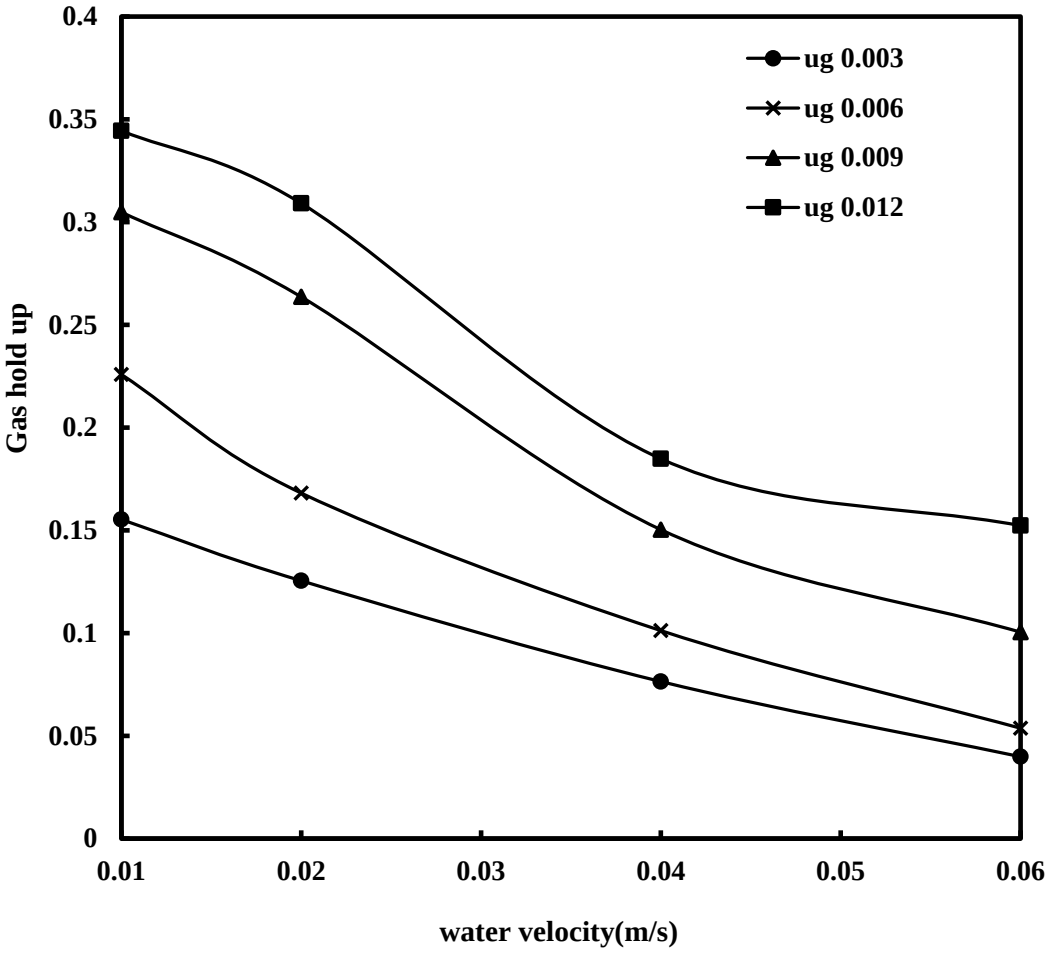

Fig 3.5 Variation of gas holdup with liquid velocity (m/s) at constant air velocities (m/s) for 8 mm Polypropylene beads at Hs= 0.247 m and grid size 0.005m using laminar model.

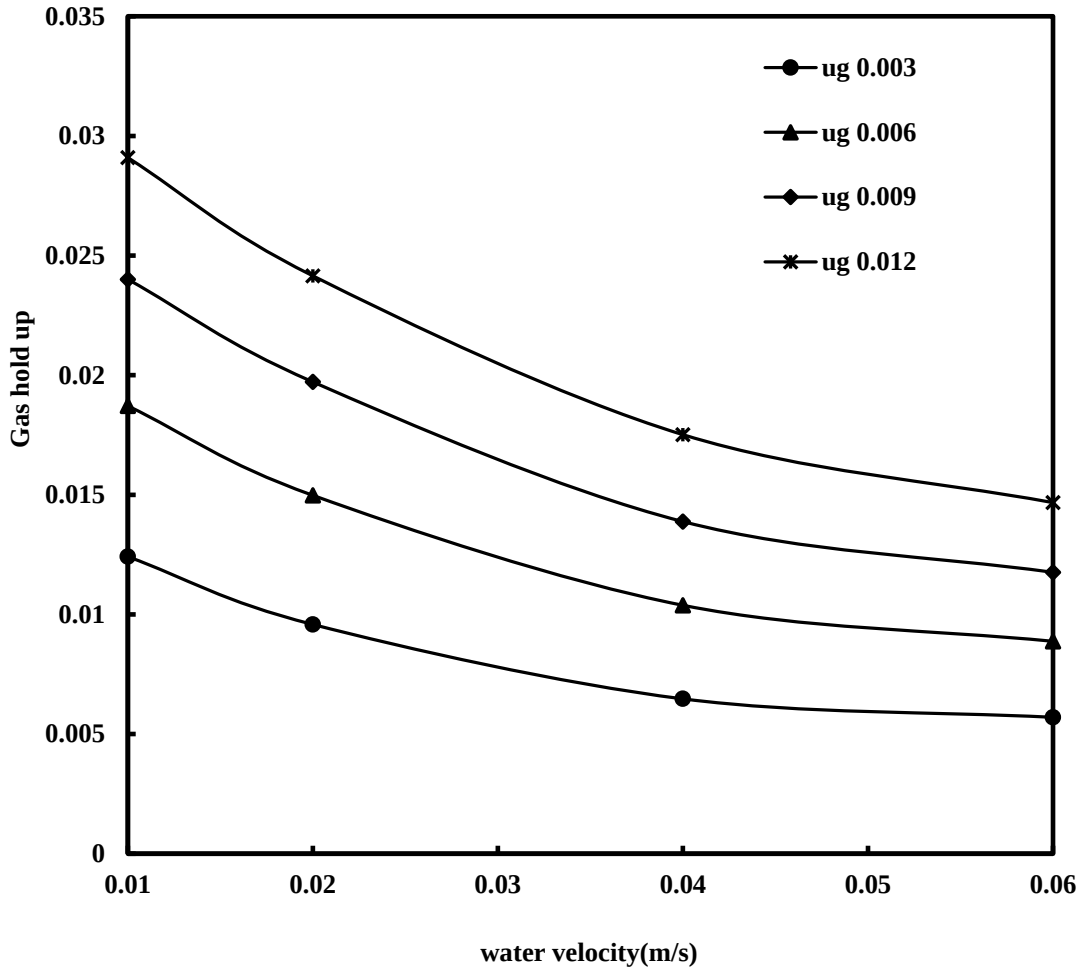

Fig 3.6 Variation of gas holdup with liquid velocity (m/s) at constant air velocities (m/s) for 8 mm Polypropylene beads at Hs= 0.247 m and grid size 0.0075m using laminar model.

Fig 3.7 and 3.8 shows that the comparison of laminar and turbulent model at a constant gas velocity. It has been seen that the lines of viscous laminar and turbulent model (k-epsilon) obtained from plot of gas hold up to water velocity, the obtained lines are quite overlapping to each other. Or shows very similar behavior. It also shows that at lower water velocity the value of gas holdup is higher and as the water velocity increases gas hold up start to decrease. The comparison graph also shows that, at constant gas velocity the values of bed pressure drop is higher in viscous laminar model compare to turbulent model (k-epsilon).

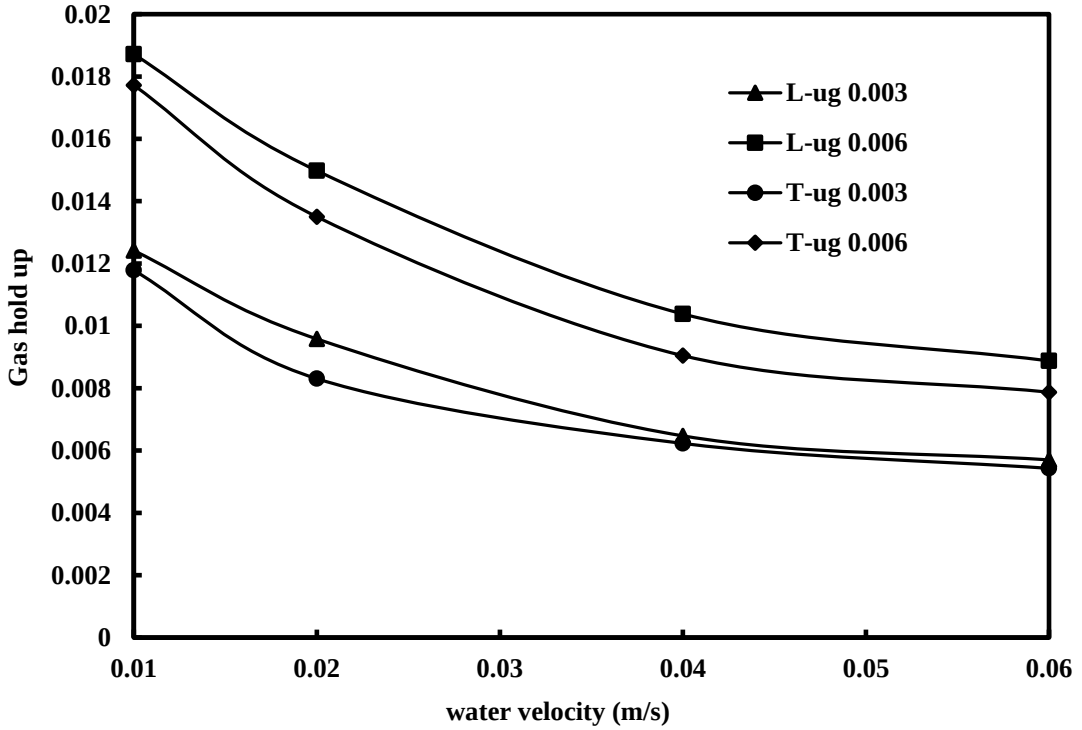

Fig 3.7 Comparison of gas holdup between laminar and turbulent model with liquid velocity (0.01 to 0.06m/s) at constant air velocities (m/s) for 8 mm Polypropylene beads at Hs= 0.247 m and grid size 0.0075m.

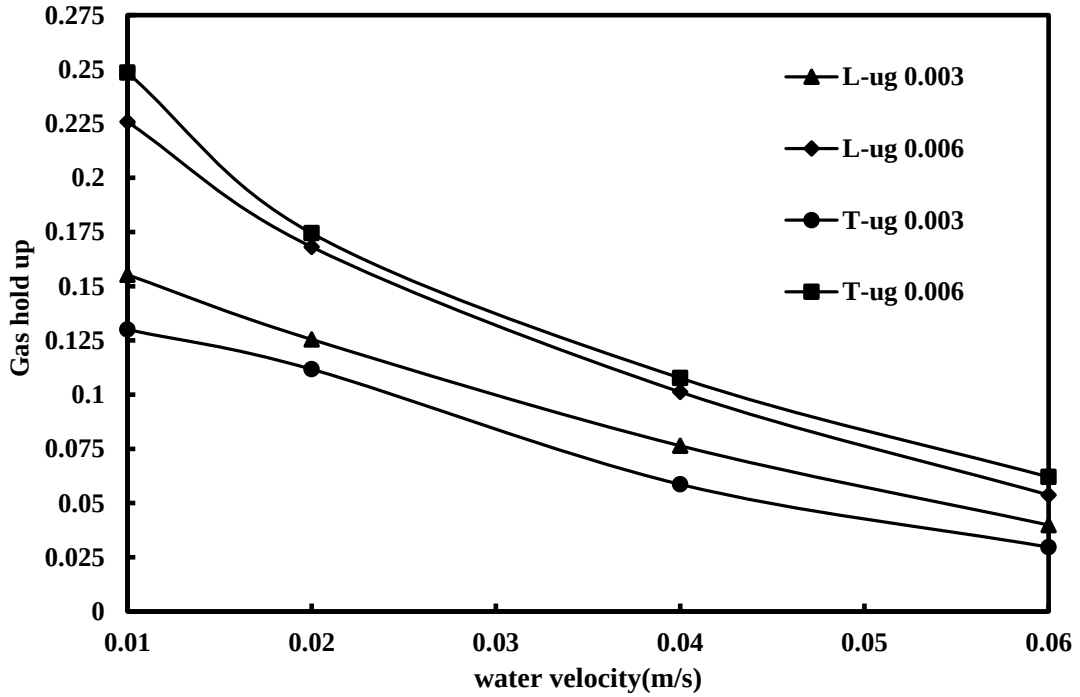

Fig 3.8 Comparison of gas holdup between laminar and turbulent model with liquid velocity (0.01and 0.06m/s) at constant air velocities (m/s) for 8 mm Polypropylene beads at Hs= 0.247 m and grid size 0.005m.

In Fig 3.9 it shows the grid indecency of laminar model at constant gas velocity. Grid size of 0.005 and 0.0075m have been taken in to problem. Changing the grid size means changing the number of elements and nodes, if we go for lower grid size (0.005m) the number of nodes and elements are larger than the 0.0075m grid size, hence more number of nodes and element take more time to simulate but it has more accuracy than lower grid size.

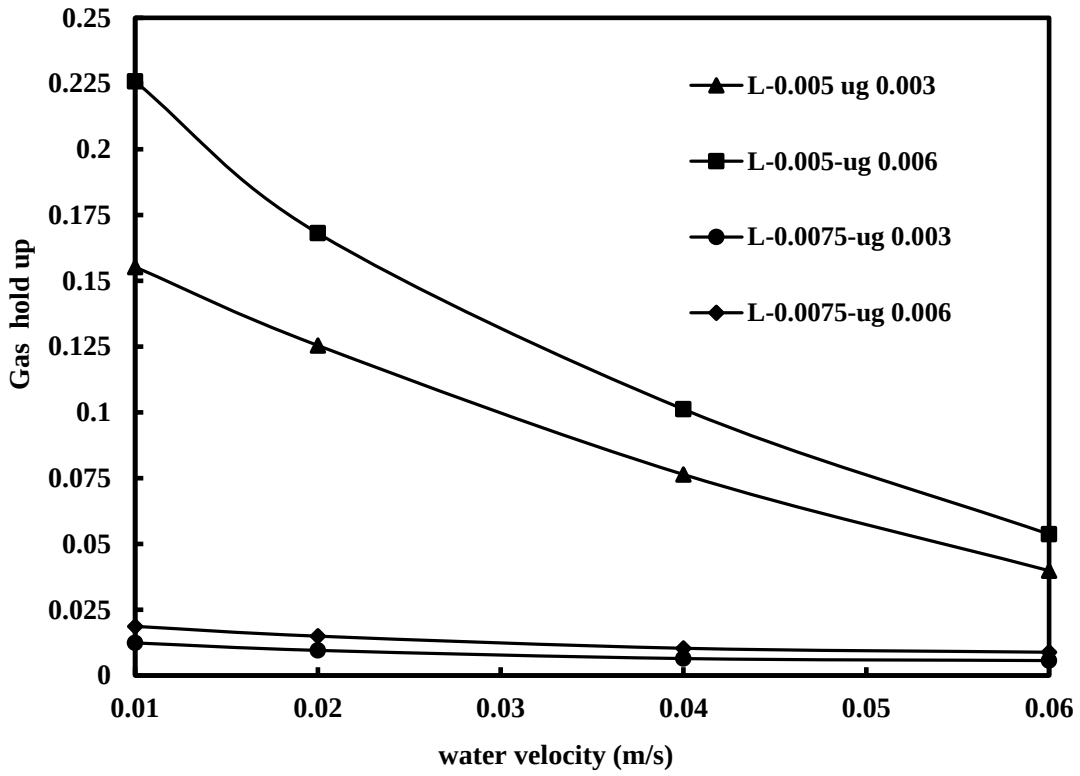

Fig 3.9 Comparison of air hold up between grid size 0.005-0.0075m with liquid velocity (0.01 to 0.06m/s) at constant air velocities (m/s) for 8 mm Polypropylene beads at H_s= 0.247 m with laminar model.

Bed height: Bed starts to expand when the fluid velocity is higher than the minimum fluidization velocity. The minimum fluidization velocity is obtained when the buoyancy force working on the particle has been balanced by the weight of the particle, after that bed starts to fluidise, this condition is also known as minimum condition for fluidization When the bed starts to fluidized XY plot of bed height to liquid velocity shows that the bed height expands when the fluid velocity increases. The graph also shows that at constant water velocity bed expansion occurs due to increase in gas velocity.

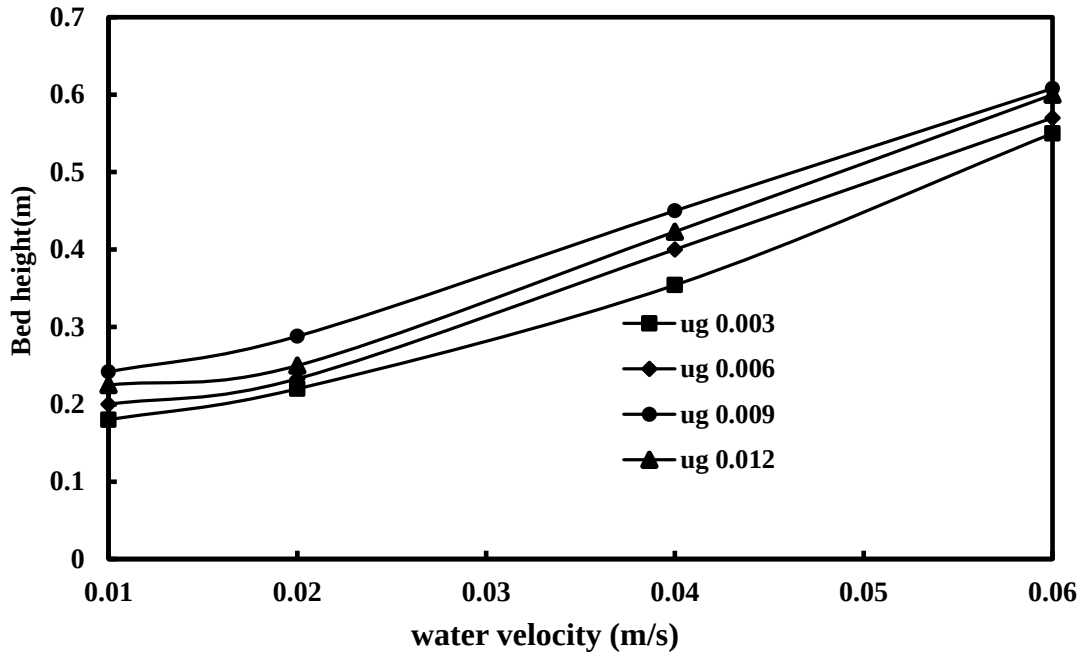

Fig 3.10 Variation of bed height (m) with liquid velocities (m/s) at constant gas velocities (m/s) for 8 mm polypropylene beads at Hs= 0.247m, grid size 0.0075m and laminar model.

Fig 3.10 is the comparison of bed height variations in two different modeling viscous laminar and turbulent (k-epsilon). Data has been obtained and plotted in XY. Plotted data shows that the behavior of laminar and turbulent are not much of different, which shows that for my current operating conditions we have liberty to choose any of the model because they both show similar behavior.

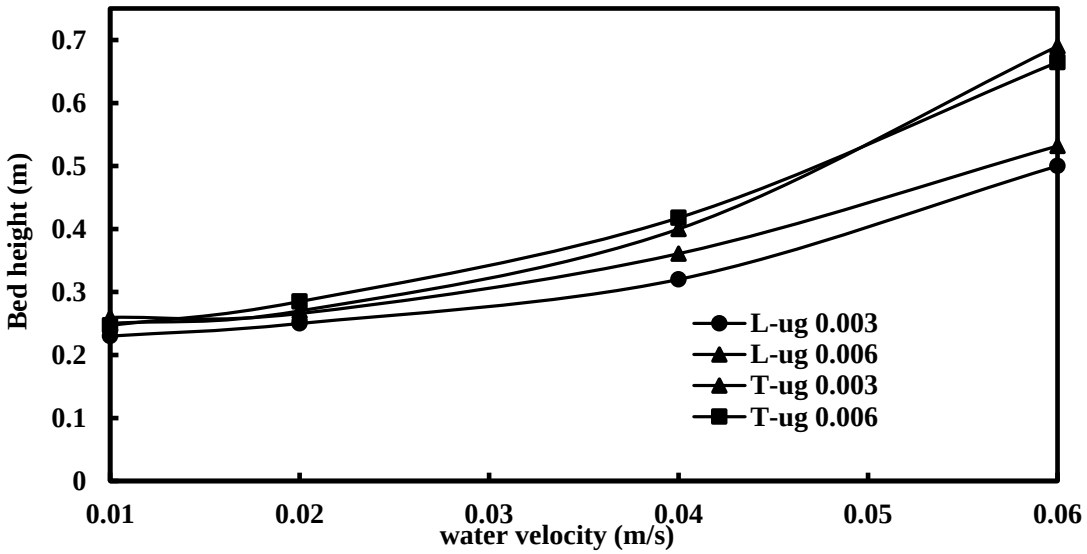

Fig 3.11 Comparison of bed height between laminar and turbulent model with liquid velocity (0.01 to 0.06m/s) at constant air velocities (m/s) for 8 mm Polypropylene beads at Hs= 0.247 m and grid size 0.0075m.

Chapter 4

Conclusion and future work

CFD simulation of hydrodynamics of gas-fluid-solid fluidized bed have been carried out for distinctive working conditions by utilizing the Eulerian-Eulerian granular multiphase methodology. The hydrodynamic parameters contemplated are gas hold up, bed extension and bed pressure drop. Distinctive examination diagrams have been indicated underneath for the dissection of progress gas hold up, bed expansion and bed pressure drop in different models (laminar and turbulent) and different mesh sizes (0.005 and 0.0075m).

Plots of bed pressure drop vs. inlet air speed at different inlet water speed shows that bed pressure drop decreases as air speed has been increased. At constant water velocity, the bed pressure drop decreases as gas velocity increased. Additionally when the air speed is little (Ug=0.003 m/s) there is no considerable build in bed pressure drop. This could be described in that way that at very little air velocity the operation behaves liquid-solid fluidization Plots of gas hold up and fluid velocity shows that the value of gas holdup has been decreasing due to increasing in water velocity at constant gas velocity. It also shows that the gas hold up value increases in the increment of gas velocity at constant liquid velocity. When the bed starts to fluidized XY plot of bed height to liquid velocity shows that the bed height expands when the fluid velocity increases. The graph also shows that at constant water velocity bed expansion occurs due to increase in gas velocity.

Future work:

- Analysis of Impact of distributor plate on hydrodynamics properties of three-phase fluidized bed with low density solid particles needs to be done.
- CFD study on the effect of different static bed height on hydrodynamics of fluidized bed for low density material needs to be done.
- Beside Eulerian multiphase phase model, discrete phase model need to be apply to solid and gas phase.

References

Allia, K., Tahar, N., Toumi, L., Salem, Z., 2006. Biological treatment of water contamination by hydrocarbon in three-phase gas-liquid-solid fluidized bed. Global NEST Journal, Vol-8 (1), 9 – 15.

Annaland, M., S., Deen, N., G., Kuipers, J., A., M., 2005. Numerical simulation of gas–liquid–solid flows using a combined front tracking and discrete particle method. Chemical Engineering Science 60, 6188 – 6198.

Bunner, B., Tryggvason, G., 1999. Direct numerical simulations of dispersed flows. In: Proceedings of the Ninth Workshop on Two-Phase Flow Predictions, Germany, 13 – 19.

Glover G.M.C, Generalis S., C., 2004. Gas-liquid-solid flow modelling in a bubble column. Chemical Engineering and Processing 43,117 – 126.

Cao, C., Liu, M., Wen, J., Guo, Q., 2009. Experimental measurement and numerical simulation for liquid flow velocity and local phase hold-ups in the riser of a GLSCFB. Chemical Engineering and Processing: Process Intensification 48, 288 – 295.

Chen, C., Fan, L.S., 2004. Discrete Simulation of Gas-Liquid Bubble Columns and Gas-Liquid-Solid Fluidized Beds. AIChE Journal 50, 288 – 301.

Cheung, S.C.P., Yeoh, G.H., Tu, J.Y., 2007.On the numerical study of isothermal vertical bubbly flow using two population balance approaches.Chem.Eng.Sci.62, 4659 – 4674.

Feng, W., Wen, J., Fan, J., Yuan, Q., Jia, X., Sun, Y., 2005. Local hydrodynamics of gas-liquid-nanoparticles three-phase fluidization. Chemical Engineering Science 60, 6887 – 6898.

Fan, L.S., 1989. Gas-Liquid-Solid Fluidization Engineering. Butterworth Series in Chemical Engineering, Butterworth Publishers, Boston, MA.

Fluent 6.2.16. Fluent 6.2.16 User's Guide, Fluent Inc. 2004.

Rafique, M., Chen, P., Dudukovic, M., 2004. Computational modeling of gas-liquid flow in bubble columns. Reviews in Chemical Engineering 20, 225–375.

Rajasimman, M., Karthikeyan, C., 2006. Aerobic digestion of starch wastewater in a fluidized bed bioreactor with low density biomass support. Journal of Hazardous Materials 143, 82 – 86.

Schallenberg, J., Enß, J., H., Hempel, D., C., 2005. The important role of local dispersed phase hold-ups for the calculation of three-phase bubble columns. Chemical Engineering Science 60, 6027 – 6033.

Shah, Y.T., 1979. Gas-liquid-solid reactor design. McGraw-Hill, New York.

Sivaguru, K., Begum K., M., Anantharaman, N., 2009. Hydrodynamic studies on three-phase fluidized bed using CFD analysis. Chemical Engineering Journal 155, 207 – 214.

Sokół, W., Halfani, M.R., 1999.Hydrodynamics of a gas-liquid-solid fluidized bed bioreactor with a low density biomass support. Biochemical Engineering Journal 3, 185 – 192.

Sokół, W., 2001. Operating parameter for a gas-liquid-solid fluidized bed bioreactor with a low density biomass support. Biochemical Engineering Journal 8, 203 – 212.

Sokół, W., Korpal, W., 2004.Determination of the optimal operational parameters for a three-phase fluidized bed bioreactor with a light biomass support when used in treatment of phenolic waste waters. Biochemical Engineering Journal 20, 49 – 56.

Sokolichin, A., Eigenberger, G., Lapin, A., 2004. Simulation of buoyancy driven bubbly flow: established simplifications and open questions. AIChE Journal 50, 24 – 45.

Wild, G., Poncin, S., 1996. Chapter 1: Hydrodynamics. In: Three-Phase Sparged Reactors, Nigam, K.D.P., and Schumpe, A., ed., Gordon and Breach Publishers, Amsterdam, The Netherlands.

Wiemann, D., Mewes, D., 2005. Calculation of flow fields in two and three-phase bubble columns considering mass transfer. Chemical Engineering Science 60, 6085 – 6093.

Zhang, J., 1996. Bubble Columns and Three-Phase Fluidized Beds: Flow Regimes and Bubble Characteristics, PhD thesis, UBC, Vancouver.

Zhang, J., Li, Y., Fan, L., S., 2000a. Numerical studies of bubble and particle dynamics in a three-phase fluidized bed at elevated pressures. Powder Technology 112, 46 – 56.

Zhang, J., Li, Y., Fan, L., S., 2000b. Discrete phase simulation of gas-liquid-solid fluidization systems: single bubble rising behavior. Powder Technology 113, 310 – 326.